Hydrothermally Obtaining Superconductor Single Crystal of $FeSe_{0.2}Te_{0.8}$ without Interstitial Fe

Sheng Ma(马晟)[1,2†], Shanshan Yan(闫珊珊)[3†], Jiali Liu(刘家利)[1,2], Yizhe Wang(王怡哲)[3], Yuhang Zhang(张宇航)[1,2], Zhen Zhao(赵振)[1,2], Zouyouwei Lu(鲁邹有为)[1,2], Dong Li(李栋)[1], Yue Liu(刘樾)[1,2], Jihu Lu(卢佶虎)[1,2], Hua Zhang(张华)[1,2,4], Haitao Yang(杨海涛)[1,2,5], Fang Zhou(周放)[1,2,4], Zian, Li(李子安)[3*], Xiaoli Dong(董晓莉)[1,2,4*], and Zhongxian Zhao(赵忠贤)[1,2,4]

[1]*Beijing National Laboratory for Condensed Matter Physics, Institute of Physics, Chinese Academy of Sciences, Beijing 100190, China*
[2]*School of Physical Sciences, University of Chinese Academy of Sciences, Beijing 100049, China*
[3]*School of Physical Science and Technology, Guangxi University, Nanning 530004, China*
[4]*Songshan Lake Materials Laboratory, Dongguan 523808, China*
[5]*CAS Center for Excellence in Topological Quantum Computation, University of Chinese Academy of Sciences, Beijing 100190, China*

(Received 15 April 2023; accepted manuscript online 11 May 2023)

We report a hydrothermal route to remove interstitial excess Fe in non-superconducting iron chalcogenide $Fe_{1+\delta}Se_{1-x}Te_x$ single crystals. The extra-Fe-free ($\delta \sim 0$) $FeSe_{0.2}Te_{0.8}$ single crystal thus obtained shows bulk superconductivity at $T_c \sim 13.8$ K, which is about 2 K higher than the $FeSe_{0.2}Te_{0.8}$ sample obtained by usual post-annealing process. The upper critical field $\mu_0 H_{c2}$ is estimated to be ~ 42.5 T, similar to the annealed $FeSe_{0.2}Te_{0.8}$. It is surprising to find that the hydrothermal $FeSe_{0.2}Te_{0.8}$ exhibits a remarkably small isothermal magnetization hysteresis loop at $T = 3$ K. This yields an extremely low critical current density $J_c \sim 1.1 \times 10^2$ A·cm^{-2} (over 100 times smaller than the annealed $FeSe_{0.2}Te_{0.8}$) and indicates more free vortices in the hydrothermal $FeSe_{0.2}Te_{0.8}$.

DOI: 10.1088/0256-307X/40/6/067402

The iron chalcogenide $FeSe_{1-x}Te_x$ superconductor[1] is regarded as a candidate for studying topological superconductivity[2–5] and is also promising in practical applications.[6–8] It is essential to synthesize high-quality $FeSe_{1-x}Te_x$ single crystals with bulk superconductivity for investigating the intrinsic physical properties.[9–16] The as-grown $Fe_{1+\delta}Se_{1-x}Te_x$ single crystals with the self-flux method inherently contains excess Fe atoms (δ in quantity) for Te substitution $x > 0.5$, which occupy the interstitial sites of the Fe(Se,Te) layers.[17] These interstitial irons are found to strongly suppress superconductivity and cause the physical properties to vary from sample to sample,[7,10,14,18–20] interfering with a consistent understanding of the intrinsic physics. Thermal annealing at $T \sim 400$ ℃ has been widely used to significantly mitigate or even completely remove the interstitial Fe in $Fe_{1+\delta}Se_{1-x}Te_x$.[21] The post-annealing in O_2, S, Te atmospheres or liquids can largely reduce the excess Fe, and bulk superconductivity can be realized in the $FeSe_{1-x}Te_x$ system.[20–27] However, the superconducting (SC) and normal-state properties, including the SC transition T_c, magnetic and electrical transport behavior as well as the phase diagram, are still dependent on the annealing conditions.[21,23,24,27–31] Therefrom, the annealed sample must be restricted to a small thickness of ~ 0.05 mm to ensure an efficient removing of excess Fe and guarantee the chemical/physical homogeneity and crystal quality of the sample. Therefore, improving the post-treatment technique to obtain large extra-Fe-free $FeSe_{1-x}Te_x$ superconducting single crystals is highly desirable for both the fundamental and applied studies.

In this work, we develop a soft-chemical treatment at a lower $T < 200$ ℃ based on our previous hydrothermal ion de-intercalation (HID) method[32,33] to efficiently remove the excess Fe in as-grown $Fe_{1+\delta}Se_{1-x}Te_x$ single crystals. High-quality extra-Fe-free $FeSe_{0.2}Te_{0.8}$ single crystals with dimensions up to 5 mm × 5 mm × 0.2 mm can be obtained through the HID process within a shorter period of three days. Magnetic and electrical transport measurements confirmed the bulk superconductivity with a higher $T_c \sim 13.8$ K in the HID $FeSe_{0.2}Te_{0.8}$ compared to the $FeSe_{0.2}Te_{0.8}$ obtained by post-annealing at $T \sim 400$ ℃. The upper critical field $\mu_0 H_{c2}$ estimated to be ~ 42.5 T is similar to the annealed $FeSe_{0.2}Te_{0.8}$ sample. Surprisingly, the HID $FeSe_{0.2}Te_{0.8}$ exhibits a remarkably small isothermal magnetization hysteresis loop at 3 K, which yields a very low critical current density $J_c \sim 1.1 \times 10^2$ A·cm^{-2} that is two orders of magnitude smaller than the thermally annealed counterpart. Such a small-J_c HID $FeSe_{0.2}Te_{0.8}$ may provide a superior platform for an in-depth study of the topology superconductivity, especially the issue of whether the Majorana zero modes ride on the free vortex or impurity-assisted vortex.[34–36]

Experiments. Carefully selected large high-quality $Fe_{1+\delta}Se_{0.2}Te_{0.8}$ single crystals grown by self-flux method were used as the precursors for the hydrothermal treatment. The $Fe_{1+\delta}Se_{0.2}Te_{0.8}$ precursors were usually non-superconducting, sometimes showed weak superconductivity, which had no detectable influence on the final physical properties of the resultant HID samples. Fe pow-

†These authors contributed equally to this work.
*Corresponding authors. Email: zianli@gxu.edu.cn; dong@iphy.ac.cn
© 2023 Chinese Physical Society and IOP Publishing Ltd

der (Alfa Aesar, 99.998% purity) of 0.02 mol and selenourea (Alfa Aesar, 99% purity) of 0.02 mol were used as the hydrothermal reagents. The HID reactions were performed in stainless steel autoclaves of 25 ml capacity with Teflon liners.[32,33] The autoclave loaded with the precursors, reagents and 5 ml deionized water was tightly sealed and heated at 150–200 ℃ for three days. The obtained extra-Fe-free $FeSe_{0.2}Te_{0.8}$ single crystals, about 5 mm × 5 mm × 0.2 mm in dimensions, were washed by deionized water. For comparison, the $Fe_{1+\delta}Se_{0.2}Te_{0.8}$ precursors were also annealed in Te vapor at 400 ℃ for five days.[21] The crystal structure and microstructure, morphology, chemical composition, and the superconducting properties of the HID and annealed $FeSe_{0.2}Te_{0.8}$ single crystals were carefully characterized. X-ray diffraction was carried out at room temperature on a Rigaku Ultima Ⅳ (3 kW) diffractometer using Cu K_α radiation, with a 2θ range of 10°–80° and a scanning step of 0.01°. X-ray rocking curve was measured on a diffractometer (Rigaku SmartLab, 9 kW) equipped with two Ge (220) monochromators. The superconducting diamagnetic signals were measured on a Quantum Design MPMS-XL1 system with a tiny remnant field <4 mOe. The field-dependent magnetization measurements were conducted on a Quantum Design MPMS-3 system. The electrical resistivity was measured on a Quantum Design PPMS-14 system. The microstructure analysis was performed on a transmission electron microscope (TEM, ARM200F, JEOL Ltd.) equipped with both probe and image aberration correctors (CEOS GmbH). While a non-stoichiometric amount of Fe (δ in excess) is obvious in $Fe_{1+\delta}Se_{0.2}Te_{0.8}$ precursors based on inductively coupled plasma atomic emission spectroscopy and scanning electron microscopy, no such interstitial Fe is detectable in both the final HID and annealed $FeSe_{0.2}Te_{0.8}$ samples within the instrumental resolution.

Results and Discussion. Figure 1(a) is a schematic illustration of the HID method, by which the interstitial Fe in as-grown $Fe_{1+\delta}Se_{1-x}Te_x$ precursor (FST-As) can be completely removed, while the host crystal structure remains unchanged. Figure 1(b) shows the XRD pattern of the HID $FeSe_{0.2}Te_{0.8}$ (FST-HID) single crystal, exhibiting a single set of {001} reflections. The full width at half maximum (FWHM) of x-ray rocking curve is about 0.11° for the (005) Bragg reflection of FST-HID [Fig. 1(c)], indicating a high-quality crystalline structure of the sample.

The morphology and microstructure features of the samples were investigated using transmission electron microscopy (TEM). Figures 2(a)–2(c) display the typical bright-field TEM images of the as-grown (FST-As), annealed (FST-An), and hydrothermal (FST-HID) specimens, respectively. The common feature in the TEM images is the occurrence of herringbone-like contrast, which can be recognized as the formation of dislocation networks in the FST-As, FST-An, and FST-HID samples. The density and distribution of dislocation networks are similar among the three samples. Figures 2(d), 2(e), and 2(f) show the zone-axis [001]-oriented electron diffraction patterns of the FST-As, FST-An, and FST-HID samples, respectively. The sharp diffraction spots indicate the high-quality single crystals, in consistence with the XRD results (Fig. 1). Interestingly, the networks of dislocations in these specimens do not obviously affect the corresponding electron diffraction patterns [Figs. 2(d)–2(f)] taken from the dislocation-infested regions, owing to the limited volume of the line defective nature of dislocations. However, a close inspection of these diffraction patterns reveals that very weak reflections of $\{h\,k\,0\}$ (h or k is odd) appear for FST-As [Fig. 2(d)]. This may be due to the small separation in the occupancy, or preference of sites of Te and Se atoms, which leads to the difference between the atomic scattering factors as reported previously.[11] It is worthy of noting that Fig. 2(d) also displays a clear diffuse scattering background between the diffraction spots, which can be attributed to the interstitial excess Fe in FST-As. The diffuse scatterings are significantly mitigated for FST-An [Fig. 2(e)] and FST-HID [Fig. 2(f)], indicating that the interstitial Fe atoms have been largely removed from the host lattice by the thermal annealing or hydrothermal treatment.

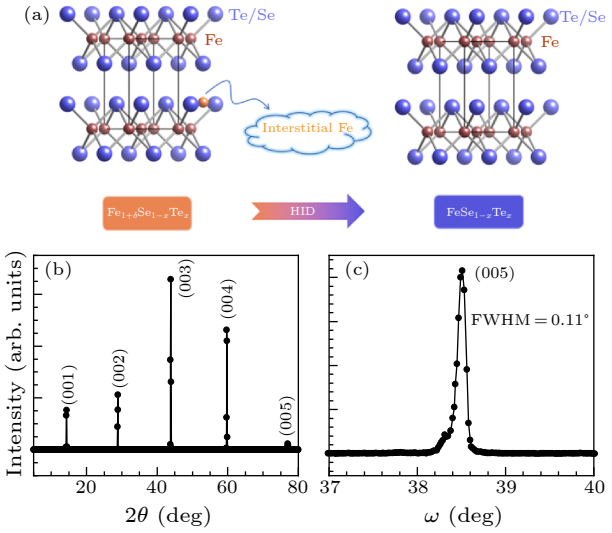

Fig. 1. (a) Schematic illustration of the hydrothermal ion-de-intercalation (HID) method for removing interstitial Fe (δ in excess) in as-grown $Fe_{1+\delta}Se_{1-x}Te_x$ single crystals. (b) XRD pattern of HID $FeSe_{0.2}Te_{0.8}$ single crystal shows a single preferred {00l} orientation. (c) Double-crystal XRD rocking curve of the HID sample gives an FWHM of 0.11° for (005) reflection, demonstrating its high crystal quality.

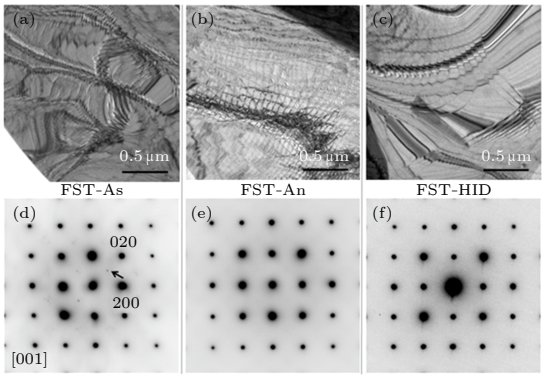

Fig. 2. Typical bright-field TEM images of (a) the as-grown FST-As, (b) the annealed FST-An and (c) the hydrothermal FST-HID specimens. The herringbone-like contrasts in (a)–(c) are associated with the dislocation networks in the specimens. (d)–(f) Their corresponding electron diffraction patterns taken along [001] zone-axis. Note that forbidden reflections of $(h, k, 0)$ with odd h, k are observed in (d) as denoted by arrow.

Magnetic susceptibility $\chi(T)$ and electrical resistivity $\rho(T)$ were measured to characterize the superconductivity of the samples. All magnetic susceptibilities were collected under an applied field H of 1 Oe with H along the crystallographic c-axis ($H//c$) after zero-field cooling. As seen in Fig. 3(a), the susceptibility curve of the as-grown FST-As sample with significant interstitial Fe atoms shows no superconductivity. In contrast, the hydrothermal FST-HID and annealed FST-An single crystals both exhibit sharp superconducting diamagnetic transition at $T_c \sim 13.8$ K and 11.4 K, respectively, and 100% superconducting shielding signal, indicating their bulk superconductivity. Figures 3(b) and 3(c) show the respective $\rho(T)$ curves of FST-An and FST-HID samples measured under $H\|c$ from 0 to 14 T by a step of 1 T. The upper critical field $\mu_0 H_{c2}(T)$ can be obtained from their $\rho(T)$ curves [Figs. 3(b) and 3(c)] using the criterion of 10% normal-state resistivity. In Fig. 3(d), the solid curves are the fits to the $\mu_0 H_{c2}(T)$ data using the two-band model,[37] yielding the $\mu_0 H_{c2}(T)$ values of ~ 42.5 T and ~ 49.5 T for FST-HID and FST-An samples, respectively. The coherence lengths of FST-HID and FST-An, ξ_{ab}, are estimated to be 2.8 nm and 2.6 nm, respectively. It has been reported that the physical properties and superconducting volume are extremely sensitive to the presence of excess Fe; a small number of interstitial irons will largely reduce the SC volume and alter the superconducting and normal-state properties.[1,14,19,21] The 100% superconducting shielding together with the higher T_c and similar $\mu_0 H_{c2}$ achieved in the hydrothermal FST-HID samples in turn evidences an efficient elimination of the interstitial Fe from the as-grown FST-As by the HID treatment, consistent with the TEM observations mentioned above.

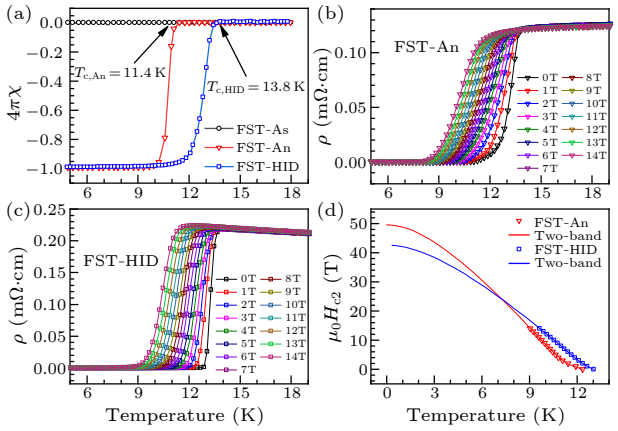

Fig. 3. (a) Temperature-dependent magnetic susceptibility near the superconducting transitions for as-grown (FST-As), annealed (FST-An), and HID (FST-HID) single crystals. The data were measured in zero-field cooling mode with $H = 1$ Oe and corrected for demagnetization factor. [(b), (c)] The resistivity $\rho(T)$ curves under $H\|c$ up to 14 T for the FST-An and FST-HID samples, respectively. (d) The temperature dependence of upper critical field $\mu_0 H_{c2}(T)$ obtained from the $\rho(T)$ data at the 10% normal-state resistivity for FST-An (red) and FST-HID (blue), fitted by the two-band model.

While the upper critical fields $\mu_0 H_{c2}$ of FST-HID and FST-An exhibit similar temperature-dependent behavior, their field-dependent magnetization $M(H)$ are very different. As shown in Fig. 4(a), the annealed FST-An sample displays symmetric isothermal magnetization hysteresis loops (MHLs) at different temperatures, with a clearly visible second peak in $M(H)$. The maximum magnetization of FST-An can reach a value up to 8×10^{-2} emu/mg at $T = 3$ K. The critical current density J_c is estimated to be 7×10^4 A·cm^{-2} by the Bean model.[38,39] Both the MHLs and the J_c value of the FST-An sample are consistent with the previous reports.[21] In contrast, the hydrothermal FST-HID sample shows a set of abnormal MHLs. Firstly, as shown in Fig. 4(b), the isothermal MHLs are remarkably depressed compared to the FST-An sample, and no peak appears in the $M(H)$ curves. Secondly, the maximum magnetization at 3 K is merely 6×10^{-4} emu/mg, accordingly yielding a small J_c of 1.1×10^2 A·cm^{-2}, which is two orders of magnitude smaller than that of FST-An. Such small dimension of MHLs indicates that vortex pinning effect by impurities is extremely weak, implying that free vortices are dominant in the FST-HID sample. Thirdly, unlike annealed FST-An, the MHLs of FST-HID are obviously asymmetric. To our knowledge, such a low J_c with asymmetric MHLs is rare in unconventional bulk superconductors, which deserves further investigation.

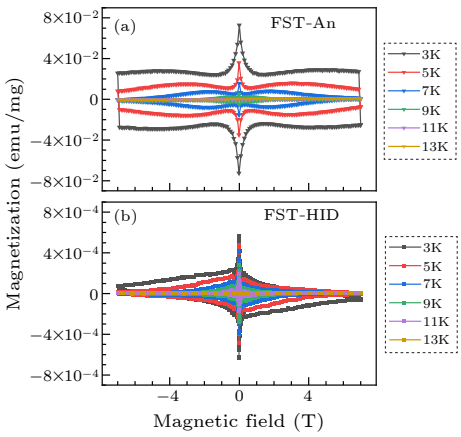

Fig. 4. Magnetization hysteresis loops measured under external field applied along c-axis for (a) FST-An and (b) FST-HID samples. The background signal from sample holder was subtracted for the FST-HID sample. Note that the magnetization scale in (b) is two orders of magnitude smaller than that in (a).

In summary, we succeed in eliminating the interstitial Fe in as-grown non-superconducting $Fe_{1+\delta}Se_{1-x}Te_x$ single crystal through a soft-chemical hydrothermal treatment. The obtained extra-Fe-free $FeSe_{0.2}Te_{0.8}$ single crystal shows bulk superconductivity at $T_c \sim 13.8$ K, which is about 2 K higher than the $FeSe_{0.2}Te_{0.8}$ sample obtained by post annealing. The upper critical field $\mu_0 H_{c2}$ is estimated to be ~ 42.5 T, similar to the annealed sample. Surprisingly, the hydrothermal $FeSe_{0.2}Te_{0.8}$ exhibits remarkably small isothermal MHLs and correspondingly a very low J_c value that is more than 100 times smaller than the thermally annealed counterpart. This implies that the vortex pinning effect due to impurities is extremely weak in the hydrothermal $FeSe_{0.2}Te_{0.8}$ sample. Our further experiments indicate that a series of $FeSe_{1-x}Te_x$ ($x > 0.5$) single crystals without interstitial Fe can be obtained by this hydrothermal treatment. These hydrothermal samples may serve as an ideal platform to further investigate the complicated physics of spin orbital coupling, topological state,

and superconductivity that are entwined in $FeSe_{1-x}Te_x$ system.

Acknowledgments. This work was supported by the National Natural Science Foundation of China (Grant Nos. 12061131005, 11974019, 11834016, and 11888101), the National Key Research and Development Program of China (Grant Nos. 2022YFA1403900), the Strategic Priority Research Program of Chinese Academy of Sciences (Grant Nos. XDB33010200 and XDB25000000), and the Chinese Academy of Sciences through the Youth Innovation Promotion Association (Grant No. 2022YSBR-048).

References

[1] Fang M H, Pham H M, Qian B, Liu T J, Vehstedt E K, Liu Y, Spinu L, and Mao Z Q 2008 *Phys. Rev. B* **78** 224503
[2] Yin J X, Wu Z, Wang J H, Ye Z Y, Gong J, Hou X Y, Shan L, Li A, Liang X J, Wu X X, Li J, Ting C S, Wang Z Q, Hu J P, Hor P H, Ding H, and Pan S H 2015 *Nat. Phys.* **11** 543
[3] Wang D F, Kong L Y, Fan P, Chen H, Zhu S Y, Liu W, Cao L, Sun Y J, Du S X, Schneeloch J, Zhong R, Gu G, Fu L, Ding H, and Gao H J 2018 *Science* **362** 333
[4] Zhang P, Yaji K, Hashimoto T, Ota Y, Kondo T, Okazaki K, Wang Z, Wen J, Gu G D, Ding H, and Shin S 2018 *Science* **360** 182
[5] Zhao H, Li H, Dong L, Xu B, Schneeloch J, Zhong R, Fang M, Gu G, Harter J, Wilson S D, Wang Z, and Zeljkovic I 2021 *Nat. Phys.* **17** 903
[6] Hosono H, Yamamoto A, Hiramatsu H, and Ma Y 2018 *Mater. Today* **21** 278
[7] Si W D, Han S J, Shi X Y, Ehrlich S N, Jaroszynski J, Goyal A, and Li Q 2013 *Nat. Commun.* **4** 1347
[8] Liu X, Wei S, Shi Y, Liu F, Zhou C, Li Q, Li Y, Liu L, Shi Z, Ren L, Xu Y, Duan P, Yang Z, Ge J, Qi Y, Song Y, Liu H, Zhang Z, and Qin J 2022 *Supercond. Sci. Technol.* **35** 10LT01
[9] Lei H C, Hu R W, Choi E S, Warren J B, and Petrovic C 2010 *Phys. Rev. B* **81** 094518
[10] Bendele M, Babkevich P, Katrych S, Gvasaliya S N, Pomjakushina E, Conder K, Roessli B, Boothroyd A T, Khasanov R, and Keller H 2010 *Phys. Rev. B* **82** 212504
[11] Hu H F, Zuo J M, Wen J S, Xu Z J, Lin Z W, Li Q, Gu G D, Park W K, and Greene L H 2011 *New J. Phys.* **13** 053031
[12] Okazaki H, Watanabe T, Yamaguchi T, Kawasaki Y, Deguchi K, Demura S, Ozaki T, J D S, Mizuguchi Y, Takeya H, and Takano Y 2012 *J. Phys. Soc. Jpn.* **81** 113707
[13] Dong L, Zhao H, Zeljkovic I, Wilson S D, and Harter J W 2019 *Phys. Rev. Mater.* **3** 114801
[14] Sun Y, Shi Z, and Tamegai T 2019 *Supercond. Sci. Technol.* **32** 103001
[15] Eguchi R, Senda M, Uesugi E, Goto H, Fujiwara A, Imai Y, Kimura S, Noji T, Koike Y, and Kubozono Y 2020 *Mater. Res. Express* **7** 036001
[16] Sun Y, Pan Y, Zhou N, Xing X, Shi Z, Wang J, Zhu Z, Sugimoto A, Ekino T, Tamegai T, and Kitano H 2021 *Phys. Rev. B* **103** 224506
[17] Bao W, Qiu Y, Huang Q, Green M A, Zajdel P, Fitzsimmons M R, Zhernenkov M, Chang S, Fang M, Qian B, Vehstedt E K, Yang J, Pham H M, Spinu L, and Mao Z Q 2009 *Phys. Rev. Lett.* **102** 247001
[18] Liu T J, Ke X, Qian B, Hu J, Fobes D, Vehstedt E K, Pham H, Yang J H, Fang M H, Spinu L, Schiffer P, Liu Y, and Mao Z Q 2009 *Phys. Rev. B* **80** 174509
[19] Sales B C, Sefat A S, Mcguire M A, Jin R Y, Mandrus D, and Mozharivskyj Y 2009 *Phys. Rev. B* **79** 094521
[20] Komiya S, Hanawa M, Tsukada I, and Maeda A 2013 *J. Phys. Soc. Jpn.* **82** 064710
[21] Sun Y, Tsuchiya Y, Yamada T, Taen T, Pyon S, Shi Z, and Tamegai T 2013 *J. Phys. Soc. Jpn.* **82** 093705
[22] Dong C, Wang H, Li Z, Chen J, Yuan H Q, and Fang M 2011 *Phys. Rev. B* **84** 224506
[23] Hu J, Wang G C, Qian B, and Mao Z Q 2012 *Supercond. Sci. Technol.* **25** 084011
[24] Kawasaki Y, Deguchi K, Demura S, Watanabe T, Okazaki H, Ozaki T, Yamaguchi T, Takeya H, and Takano Y 2012 *Solid State Commun.* **152** 1135
[25] Koshika Y, Usui T, Adachi S, Watanabe T, Sakano K, Simayi S, and Yoshizawa M 2013 *J. Phys. Soc. Jpn.* **82** 023703
[26] Friederichs G M, Wörsching M P B, and Johrendt D 2015 *Supercond. Sci. Technol.* **28** 095005
[27] Otsuka T, Hagisawa S, Koshika Y, Adachi S, Usui T, Sasaki N, Sasaki S, Yamaguchi S, Nakanishi Y, Yoshizawa M, Kimura S, and Watanabe T 2019 *Phys. Rev. B* **99** 184505
[28] Liu T J, Hu J, Qian B, Fobes D, Mao Z Q, Bao W, Reehuis M, Kimber S A J, Prokeš K, Matas S, Argyriou D N, Hiess A, Rotaru A, Pham H, Spinu L, Qiu Y, Thampy V, Savici A T, Rodriguez J A, and Broholm C 2010 *Nat. Mater.* **9** 718
[29] Liu Y, Kremer R K, and Lin C T 2010 *Europhys. Lett.* **92** 57004
[30] Hu J, Liu T J, Qian B, and Mao Z Q 2013 *Phys. Rev. B* **88** 094505
[31] Liu L, Mikami T, Takahashi M, Ishida S, Kakeshita T, Okazaki K, Fujimori A, and Uchida S 2015 *Phys. Rev. B* **91** 134502
[32] Yuan D, Huang Y, Ni S, Zhou H, Mao Y, Hu W, Yuan J, Jin K, Zhang G, Dong X, and Zhou F 2016 *Chin. Phys. B* **25** 077404
[33] Ni S, Hu W, Shen P, Wei Z, Liu S, Li D, Yuan J, Yu L, Jin K, Zhou F, Dong X, and Zhao Z 2019 *Chin. Phys. B* **28** 127401
[34] Liu Q, Chen C, Zhang T, Peng R, Yan Y J, Wen C H P, Lou X, Huang Y L, Tian J P, Dong X L, Wang G W, Bao W C, Wang Q H, Yin Z P, Zhao Z X, and Feng D L 2018 *Phys. Rev. X* **8** 041056
[35] Li G, Zhu S, Fan P, Cao L, and Gao H J 2022 *Chin. Phys. B* **31** 080301
[36] De Mendonça B S, Manesco A L R, Sandler N, and Dias da Silva L G G V 2022 *Phys. Rev. B* **107** 184509
[37] Gurevich A 2003 *Phys. Rev. B* **67** 184515
[38] Bean C P 1964 *Rev. Mod. Phys.* **36** 31
[39] Gyorgy E M, Van Dover R B, Jackson K A, Schneemeyer L F, and Waszczak J V 1989 *Appl. Phys. Lett.* **55** 283